RSC Advances

ROYAL SOCIETY OF CHEMISTRY

www.rsc.org/advances

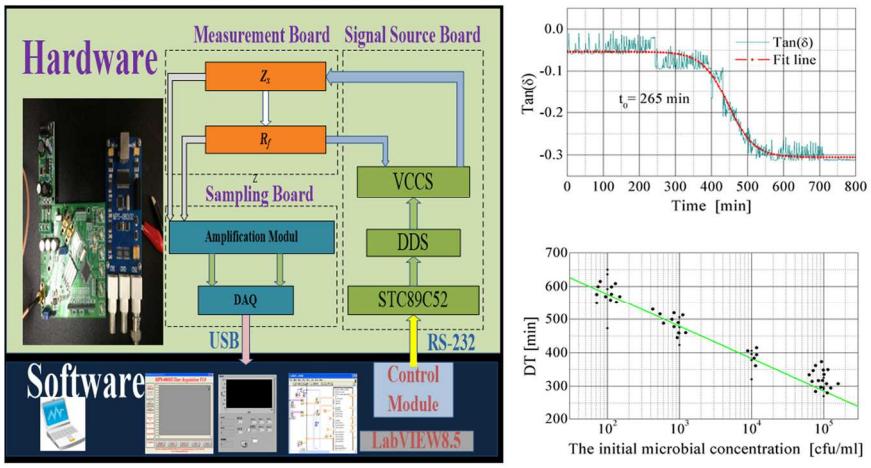

Graphical Abstract
150x79mm (300 x 300 DPI)

Dielectric Loss Angle Based Portable Biosensor System for Bacterial Concentration Detection

Jingyao Chen[1], Jie Cai[2], Xingjian Huang[1], Tian Yi[3], Kexing Wang[1], Siyi Pan[1*]

[1] *College of Food Science and Technology, Huazhong Agricultural University, Wuhan 430070, China*

[2] *College of Food Science and Engineering, Wuhan Polytechnic University, Wuhan 430023, China*

[3] *Hubei Academy of Agricultural Sciences, Wuhan 430064, Hubei, China*

[*] Corresponding author, Prof. Siyi Pan, E-mail: siyipan@outlook.com;

pansiyi@mail.hzau.edu.cn (S. Pan)

Abstract: A new type of portable sensor is proposed to detect bacterial concentration based on the change in dielectric loss angle δ. The performance of the sensor is tested in four types of drinks, namely, milk, orange juice, peach juice, and tomato juice. Notably, the sensor can detect δ when the bacterial concentration reaches a critical threshold value (approximately 10^6 cfu/mL) by applying 1 V peak-to-peak 200 Hz sinusoidal test signal of 0.25 mA at intervals of 10 min. This work introduces a portable and low-system for rapid detection. The system is a useful tool for microbial screening in industrial and commercial environments.

Keywords: Dielectric loss angle; Impedance; Portable biosensor; Bacterial count

1. Introduction

Several novel methods have been proposed and implemented to detect pathogenic bacteria over the past decades. However, people are still threatened by various bacterial pathogens. Billions of humans, particularly those in developing countries,[1-4] are facing health risks because of the lack of screening methods for pathogenic bacteria below threshold values in drinking water. A waterborne bacterium could kill off approximately 1.8 million people worldwide (U.S. Centers for Disease Control and Prevention, Atlanta, 2006). Traditional identification methods often involve complex procedures, and expensive instruments or reagents, rendering them unsuitable for applications outside microbiology.[5-7] The rapid and reproducible testing is essential in timely pathogen detection. Molecularly imprinted polymer techniques have emerged rapidly in the past decade and they made significant effects on various fields of food safety, particularly in the rapid determination of veterinary residues, pesticide residues, and microorganisms because of their low cost, selectivity and sensitivity. [3, 4] Several research works have reported that foodborne pathogenic bacteria mainly depend on the application of impedance techniques for screening. [8, 9] To date, most biosensors remain limited for unstable antibodies and replication, such as immunosensor[10-12] , DNA-based detection[10,13-15], and surface plasmon resonance. Thus, a sensitive, rapid, easy-to-use, and cost-effective method for determining bacterial concentration must be developed.

The electrical nature and electrophysiology of bacterial cells are fundamental for developing impedance methods. An equivalent circuit is composed of resistances and capacitances for analyzing electrical properties of the microelectrode interface.[16, 17] C_i and R_i represent the double-layer interface,[18-20] and *Rm* denotes the media. *Re* and *Cm* are corresponding cell components in the tested media. C_i represents the cell membrane consisting of a lipid bilayer with many proteins, where lipid molecules are oriented with their polar groups facing outward into the aqueous environment, and whereas their hydrophobic

hydrocarbon chains are pointing inward to form the interior membrane.[21-23] The inside of a cell is complex and contains membrane-covered particulates, such as mitochondria, vacuoles, and nucleus, as well as many dissolved charged molecules.[24, 25] However, when the frequency of the applied test signal sufficiently is low (<1 MHz), C_m can be neglected, and the equivalent circuit is simply reduced to a series of resistance (R_s) and capacitances (C_s). The electrical impedance of such circuit can be expressed as $Z_s = R_s + 1/(j\omega C_s)$.[26]

Based on the Z_s equivalent circuit, the impedance significantly changes after cell attachment and spreading because of an interference with the free space above the electrode. An air-filled parallel-plate capacitor C_0 is considered as a device that stores electric charge. Capacitors vary in shape and size, but their basic configuration involves two conductors carrying equal but opposite charges. Capacitance C was found to increase experimentally when the space between the conductors is filled with dielectrics. When a dielectric material is inserted to fill the space completely between the plates, the capacitance increases to $C=\kappa_e C_0$, where κ_e is the dielectric constant.[27] The increases of capacitance in the presence of a dielectric can be explained from a molecular point of view. κ_e is a measure of the dielectric response to an external electric field. Dielectrics consist of two types, namely, polar and non-polar. Polar dielectrics, such as water, have permanent electric dipole moments, whereas non-polar dielectrics do not. Electric dipole moments can be induced by placing the materials in an externally applied electric field.[28-31]

Electrons spend a bit more time near the oxygen atom than the hydrogen atom. Water has a dielectric constant of 80, but ice 40 ^{o}C has an even higher dielectric constant of 100. Capacitance is the free charge divided by the potential difference on the plates. The average electric field produced by many tiny aligned electric dipoles is crucial to understand dielectric materials. However, the alignment is not complete because of random thermal motion. The aligned molecules then generate an electric field opposite to the applied field,

but smaller in magnitude. The electric field within the dielectric is $\underset{E}{\rightarrow}=\frac{\overrightarrow{E_0}}{\kappa_e}$.[29-32] Maxwell already discussed dielectric properties of inhomogeneous systems, wherein the presence of a conducting phase in a medium often leads to dielectric loss. Maxwell derived a formula for the equivalent reactance of such a system, and providing the following equation for the loss angle: $tan\delta = \frac{\overrightarrow{E''}}{\overrightarrow{E'}}$.

In addition to its low cost, this circuit could prevent released metal ions from producing toxic bacteria, inhibiting their growth in the sample. Compared with silver and gold electrodes that exhibit bacteriostatic properties, stainless steel electrodes exhibit nonnegative effects at low applied fields. Given the different affected electrical forces on the electrode and bulk side of the structure, the ions form a double-layer region at the electrode/electrolyte interface of the electrolyte.[32]

Electrical properties of microbial concentration, including impedance, conductivity, and surface interfacial physiology, have recently been investigated.[23, 30-32] However, the quantification of microbial concentration with dielectric loss angle (DLA) δ in the culture process has not yet been reported. The cell membrane as a constant-phase element (CPE), is instated on a capacitance to simplify the equivalent circuit. Microbial concentration constantly increases in 24 h. Thus, when a critical threshold value is reached, C_s also increases. After a 24 h culture period, the phase dielectric loss angle δ occurs in microbial doubling time. The microbial concentration can also respond with δ in detection systems. Designing a reference resistor cascades the system to obtain dielectric loss angle, which adopts a sine-cosine sequence digital demodulation. Detection of soft drinks at low frequencies exhibits phase diversity with a 36 min lag at the beginning and increases in 10^6 cfu/mL. This study describes a novel portable biosensor system for bacterial concentration detection based on the DLA. This system is simple, rapid and requires no particular

knowledge of microbiological techniques, making it particularly suitable for microbial screening during industrial mass production.

2. Experimental design

The portable biosensor-detected phase angle is mainly composed of a direct digital synthesizer (DDS) signal generator, voltage-controlled constant current source (VCCS), and DAQ card. DDS could transform the sine wave signal to the constant-current source. Thus, the contact impedance is reduced at the electrode/electrolyte interface, which is very important for system accuracy. The system design is illustrated in Figs. 1(a) and 1(b).

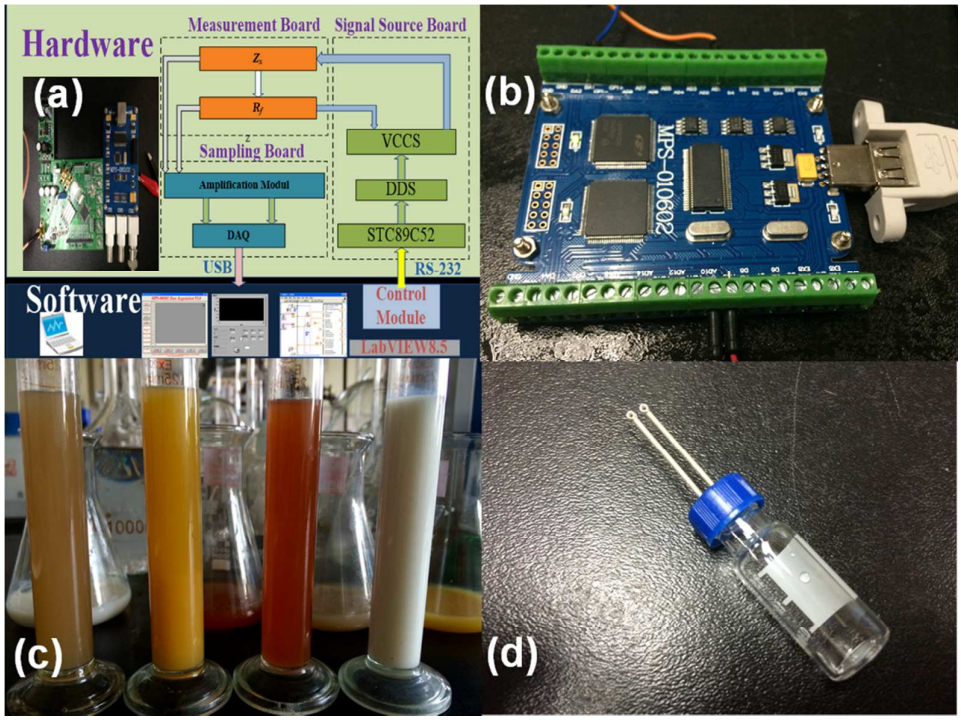

Fig. 1. Schematic (a) and photograph (b) of the biosensor system present in this work. The system is composed of an impedance measurement board, a software board and an incubation chamber containing the sample under test. Photograph (c) and photograph (d) respectively, (c)

different soft drink consists of peach juice, orange juice, tomato juice and milk. (d) The incubation chamber provided with a couple of stainless steel electrodes.

2.1 Adding sine-cosine sequence digital demodulation based on RREF

The measurement module contains two parts. Firstly, the measurement chamber features a 2 mL volume capacity. Secondly, a couple of stainless steel electrodes (conic electrodes Φ = 1 mm) is used [Fig. 2(d)]. The principle of equivalent RC circuit follows Ohm's law, in which a biological sample (adhered cell) can be treated as a resistor with resistance R and a capacitor with capacitance C connected in series. The impedance data calculated using the R and C values are based on the operating frequency[33]. Thus, impedance is complex. An algorithm is presented to calculate the impedance. Considering important differences from the algorithm using non-inverting operational amplifier (op amp), output signals from the op amp could be calculated as follows: $V_{out} = -(R_f/Z_s) \times V_{in}$, where V_{Min} and V_{Mout} could be obtained from the sinusoidal voltage signal. The frequency of a measured signal is denoted as f, and N represents the sampling points per cycle ($f_s = N \times f$). The sampled q signal cycle and the total sampling points are calculated as $M = N \times q$, given that the signal is $u(i)$. The accurate digital signal processing is dependent on twice the sampling frequency, at least for recovering the original signal impedance. The applied active electrodes and cable driver can enhance the signal-to-noise ratio and solve the problem of phase shifting, but measuring unstable phase shifting is still required in practice.[34] When θ' represents the phase shift, $\theta = \theta + \theta'$. In this work, a method input reference resistor [Fig. 2(b)] is used to eliminate error θ' in the measurement board, which is realized and verified on the platform.

The discrete Fourier transform (DFT) filter is commonly used in digital protection devices to remove the part of the signal not of interest. Voltage and current signals used in

protection devices may contain harmonics and decaying DC-offset in transient states. [35] In this case, we presented an algorithm, the orthogonal digital demodulation method, to calculate the cross-correlation functions of digital signal and digital reference sequences. This method involves adding only the sine and cosine components to the selected voltage signal by DAQ to reduce system error.

Digital signal processor (DSP) module automatically generates N points per cycle of the sequence *s(i)* of sinusoidal reference and sequence *c(i)* of cosine reference. Given the two sequences and the signal data for the correlation operation, the correlation functions R_{xrs} and R_{xrc} can be obtained. The method is as follows:

$$u(i) = A\sin(\frac{2\pi i}{N} + \theta)(i = 0,1...,M-1)$$

The test signal y(i) is changed: $y(i) = A\sin(\frac{2\pi i}{N} + \theta + \theta')(i = 0,1...,M-1)$

$$s(i) = \sin(\frac{2\pi i}{N}) \quad ; c(i) = \cos(\frac{2\pi i}{N})$$

$$R_{xrs} = \frac{1}{M}\sum_{i=0}^{M-1} y(i)\cdot s(i) = \frac{A}{2}\cos\theta - \frac{A}{2M}\sum_{i=0}^{M-1}\cos(\frac{4\pi i}{N} + \theta)$$

$$R_{xrc} = \frac{1}{M}\sum_{i=0}^{M-1} y(i)\cdot c(i) = \frac{A}{2}\sin\theta - \frac{A}{2M}\sum_{i=0}^{M-1}\sin(\frac{4\pi i}{N} + \theta)$$

$$R_{xrs} = \frac{A}{2}\cos\theta\,; R_{xrc} = \frac{A}{2}\sin\theta$$

So,

$$A = 2\sqrt{R_{xrs}^2 + R_{xrc}^2}$$

$$\theta = \arctan\frac{R_{xrc}}{R_{xrs}}$$

Supposed current was I, $Z_x = V_x I_x$; $V_r = R_r I$

So, $$Z_x = \frac{V_x}{V_r} R_r$$

$$|Z_x| = \frac{A_x}{A_r} R_r \quad ;$$

So the phase angle diversity δ, $\delta = \angle Z_x = \theta_x - \theta_r$

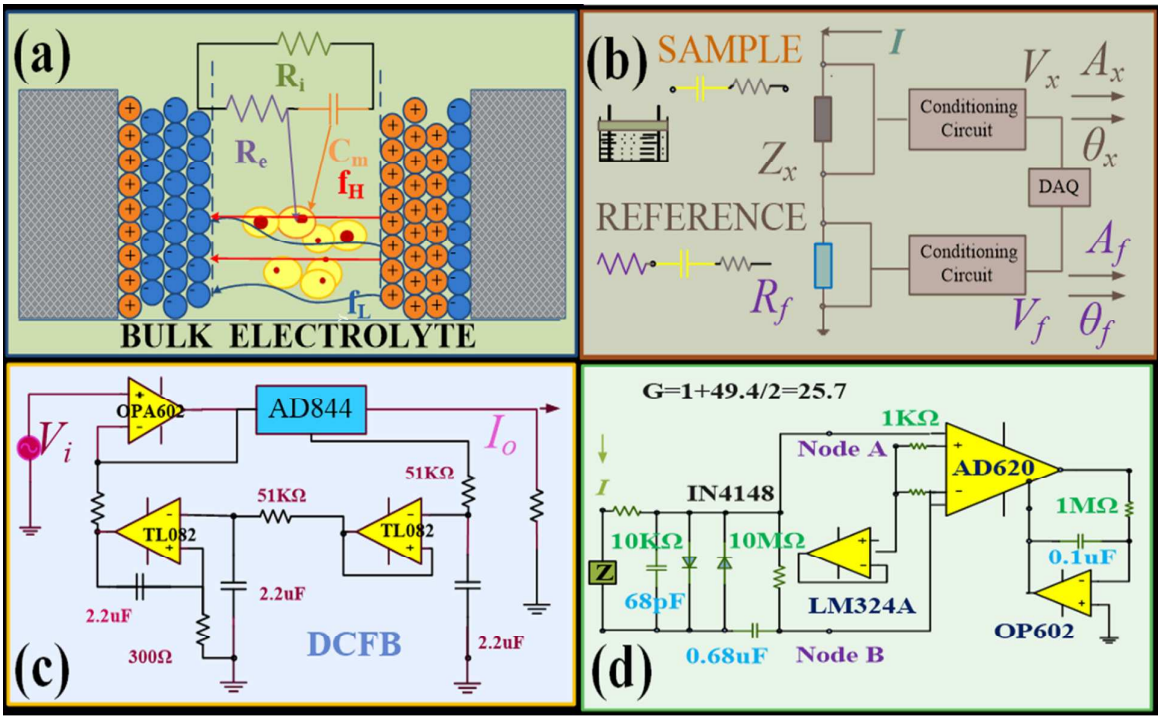

Fig.2 Front and top view (a), (b), (c) and (d) respectively, (a) Electrical model for the system electrodes-sample, the photo of the chamber in last Fig.1(d) is provided with a couple of stainless steel electrodes, electrical model for the system electrodes-sample. (b) Schematic

diagram of measuring impedance. (c) Schematic of the VCCS board (d) amplified and filtered circuit for biosensor.

2.2 VCCS mode

Ions forming a double-layer region at the electrode/electrolyte interface produce contact impedance, which affects measurement. The contact impedance should be briefly considered in relation to the effects, which reflect the authenticity of the bacterial concentration-changing discipline. Forcing a current through the known electrical model is significant because the contact impedance produced by exciting the electrode current slightly effects for a system measuring current source. The mode then measures the voltage signal. The signal source board acquires a signal switchover circuit, VCCS, which transforms voltage signal into current signal to improve measuring signal reliability. The VCCS is an electric circuit that generates a steady flow of electrons proportional to an input voltage. A low noise VCCS provides the solenoid current flow regulation necessary to generate a stable static magnetic field (B_0) [34].

Fig. 2(c) shows a schematic of the signal source board with its main components. With the development of DSP technology, DDS is adopted to generate a sine wave with high precision and stability. This sine wave is provided by the accurate sine wave signal used as the input AC signal of VCCS. The VCCS system design should solve two problems. Firstly, output impedance approach should be increased; thus, constant-current source can effectively improve the stability of its output current. Secondly, a specific process should be developed to reduce the polarization phenomenon by electrolysis and eliminate the DC component that affects the repeatability of measurements.[36, 37]

Bulk commutation technique is applied to suppress the substrate leakage current problem of CMOS rectifier.[38] The current-feedback amplifier AD844 (Analog Devices), whose internal structure is shown in Fig. 2(c) (dotted zone), is a suitable current conveyor because it reaches an internal high-impedance node for external frequency compensation. However, its gain accuracy is limited. Therefore, we built a non-inverting current circle by adding OPA602 as a voltage buffer and a series resistor R_f at the output. R_f cannot be optionally increased because the voltage at the non-inverting input must be maintained below 1 V for optimal results, depending on the feature of AD844. OPA602 could also reduce the influence of output impedance of AD844 because of its high input impedance. Moreover, to avoid saturation of the DC-blocking capacitor because of residual DC currents, the DC-feedback circuit design is a composed of second-order active filter that severs as a virtual ground for the AC signal. The actual DC voltage at the Z node is approximately 0 V. The VCCS output current is calculated as follows: $i = \frac{V_{in}}{R_f}$

2.3 Decaying DC-offset filtering [36,37]

Signal conditioning is a process of manipulating an analogue signal optimized for further processing to increase detection sensitivity. Signal conditioning has three stages, namely, filtration, amplification, and isolation. In designing these filters types determining the cut-off frequency and the stop band attenuation is important. The output from the analogue filter is fed as input into an analogue-digital converter. Fig. 2(d) shows a schematic of the signal conditioning circle and its main components. Prior to the amplification stage of signal conditioning, the signal must be filtered and optimized for DAQ reading. Filtering aimed to eliminate undesired noise from the signal of interest using passive filtering and protection circuit. The low- and high-pass passive filtering stages were designed to solve two

problems, namely, noise of electrodes and interference between hardware parts. The cut-off frequency of front-end low-pass filter was 200 kHz, where R_1 = 10 kΩ and C_1 = 68 pF. The protection circuit consisting of two diodes (IN4148) could protect signal conditioning circle and the DAQ card. The cut-off the frequency of high-pass filter was 0.05 Hz, where C_2 = 0.68 μF and R_2 = 10 MΩ. After RC filtering, an appropriate buffer could be selected for either following voltage or inverting amplifier configuration. In this part, the OP602 was chosen as a buffer amplifier for the voltage follower. This amplifier exhibited a low common-mode rejection ratio (CMRR) and was used as a driver for DAQ card input capacitance. The OP602 also illustrated signal conditioning circuitry with OPA602 and RC filters applied.

General characteristics of a differential amplifier include a low DC offset, drift, and low noise, as well as high open-loop gain, CMRR, and input impedance. In this step, AD620 (instrumentation amplifier) was selected for such purpose through the input buffer LM324A. The AD620 of 10 GΩ input impedance is suitable for applications that require a small voltage with high accuracy and minimal influence from noise. To increase resolution and SNR, the AD620 amplified the voltage by obtaining approximately 26 gain to match the reference voltage of ADC because the maximum voltage difference between A and B was 91.94 mV. The gain of instrumental amplifier was set by adjusting the resistance RG of the circuitry, where RG = 2 kΩ, with two series resistors.

2.4 Microbial analyses

At the working frequency, Z includes data from growth of equation modelled as RC circuit, whereas both types are measured separately in Z and θ.[39] In this section, based on the sensors featuring the structure depicted in Fig. 1, the experimental set-up of microbial concentration was placed in an 8 mL container [Fig. 1(d)]. The combined cultures (2 mL each) were made in a glass covered with two identical stainless steel removable electrodes. The injected current working frequency was at a density not higher than J = 1. Before each experiment, the

cultures were washed and rinsed with distilled water and sterilized at 121 °C for 20 min in an autoclave.

Given the different conserving additive amounts and sugar concentrations present in various products, we selected milk and three concentrated juices (orange, peach, and tomato). Samples of different soft drinks were also tested to monitor the microbial concentration occasionally, as well as the inoculated species. For the latter, 25 mL of each soft drinks was incubated for 24 h with automatic thermostats set at 37 °C. Gradient dilution method was then used to determine bacterial concentrations in impedance mediums.[40] Subsequently, at sterile conditions, the samples were filled with 1 mL of sterilized culture medium and 1 mL of bacterial concentrations through gradient dilution. Finally, electrodes were fixed on the samples.

3. Results and discussion

3.1 Optimal characterization analyses

This testing system should generally provide an accurate value in theoretical design and practical application. To avoid divergence decline testing accuracy, the resistance experiment was calibrated for error in the biosensor system described in Section 2. This present work reports the performance study of the sensor. Hence, characterization and subsequent standardization against the most feasible available instruments were conducted. The experiments were performed in three ways to select the sensor. The impedances of the sensors were measured (both Z and θ at the entire frequency range of 10 Hz to 125 kHz).

White Gauss noise was initially added, and the simulation results displayed an orthogonal digital demodulation algorithm with a maximum error of 0.53%. Compared with other algorithms, this method is ideal for calculating phase angle diversity. Correlation

analysis confirmed that the physical environment barely affects accuracy. At the same frequency calibrating error, the phase shift could receive accurate values of different loads. In summary, testing results indicate that the impedance, maximum error and the phase angle of the actual maximum error are <0.93%, 0.93%, and <0.03°, respectively. This method for removing the phase angle error has a high computational accuracy compared with other methods.

To validate the insensitivity of the sensor to temperature (0 °C, 15 °C, 30 °C, and 45 °C) and four humidity values (40%, 50%, 60%, and 70%), the reading was directly obtained by testing the resistor (1 kΩ). The impedance magnitude (Z) remained constant (within 1.02 kΩ - 1.06 kΩ). This finding shows that the sensor is insensitive to changes in temperature and humidity.

The phase angle with respect to the different humidity values (i.e. 40%, 50%, 60%, and 70%) and frequency as parameter is shown in Fig. 3(a). The phase angle remained constant with increasing frequency and changed in humidity [Fig. 3(a)]. Thus, the sensor is insensitive to these changes. The phase angle was consistently recorded with respect to the four temperatures for the frequency range of 10 Hz to 125 kHz [Fig. 3(b)]. The phase angle expectedly increased with frequency increasing at different temperatures [Fig. 3(b)]. This finding shows that the sensor is insensitive to changes in temperature.

To ensure the reproducibility and consistency of the sensor, each reading was repeated thrice. Data provided in Fig. 3(c) represent the average values of the three sets of reading. The phase angle of these sensors remains almost constant within the frequency range of 10 Hz to 100 kHz. The maximum error of phase was of 0.07° from 100 Hz to 50 kHz and 0.31° from 50 kHz to 100 kHz. The results indicate that the phase angle remains almost constant within 12 kHz to 20 kHz. Thus, any frequency within this bandwidth can be selected as the

sensor performance. Moreover, the system provides a 1 V peak-to-peak 200 Hz voltage test signal (V_{in}).

As previously demonstrated, the biosensor system requires a stable constant current source VCCS to ensure accuracy and stability. Logarithmic sweeping-frequency mode was used to test the RC model (R=1 kΩ, C=2.2 μF) and an excited constant current from 0.1 mA to 1.0 mA was detected at a frequency of 200 Hz [Fig. 3(d)]. Each current was tested thrice. The phase value from 0.1 mA to 0.3 mA was stable even at floating current. The deviation with increasing current density ($I \geq 0.4$ mA) is displayed. The average phase value was 6° at 0.1 mA-0.3 mA, whereas the current changed from 0.3 mA to 0.4 mA. With increasing current, electrode polarization occurs on the electrode surface. As previously indicated, this finding affects the measurement results. When the current $I > 0.3$ mA, the results assume different trends. In this work, the optimal test current used was 0.1 mA to 0.3 mA to ensure measurement accuracy. The value of impedance was obtained from 0.1 mA to 0.4 mA and was fundamentally stable even at floating current. The deviation with increasing current density ($I \geq 0.4$ mA) is displayed. Similar to the phase change, the impedance value decreased with increasing current. Given the combined effects of impedance and phase, the optimal excitation current was 0.1 mA to 0.3 mA.

The impedance magnitude also decreased with increasing frequency [Fig. 3(d)]. On the contrary, the phase angle increased with increasing frequency. In this experiment, the change curve of electrical impedance indicated different frequencies from 10 Hz to 125k Hz. The average of data were calculated. Thus, the whole test system Z was composed of electrical resistance and capacitance. The trend of the data changed at about 55 kHz, and above that frequency, considerable differences between the measured data and the Cole-Cole plot in Fig. 3(c) were found. The fitted semicircle shown in Fig. 3(c) was determined using the data between 10 and 55 kHz and the RMSE value of 0.7kΩ demonstrates that an excellent fit is

obtained within this range of frequencies.[41] However, at higher frequencies major discrepancies were found between the measured data and the Cole- Cole plot determined from low frequency data.

Specifically, when f < 1000 Hz, the test system is characterized by resistance. The magnitude impedance (Z) and phase angle of all the cases were measured using the portable biosensor in Z and θ modes to study its performance. The biosensor was excited with VCCS that supplied the content current for the system to provide accurate sampling. In these cases, 1 V peak-to-peak, 200 Hz voltage test signal (V_{in}) was provided to avoid electrode polarization effects and maintain the current at 0.25 mA.

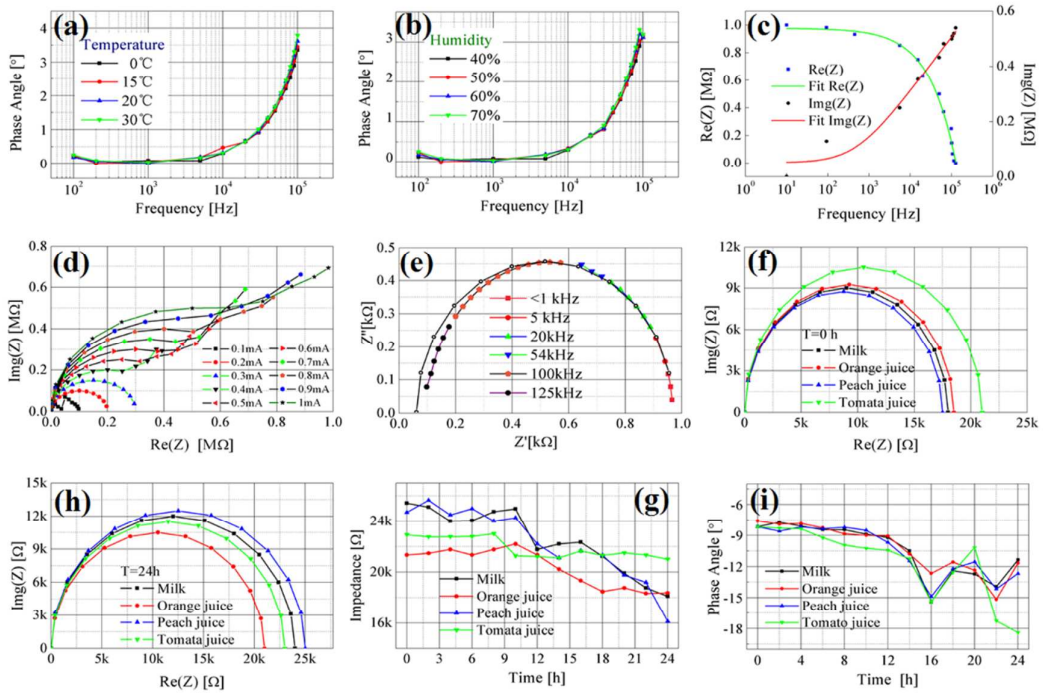

Fig.3 (a) and (b) Variation of phase angle with temperature and humidity at 10Hz to 125kHz, R=10kΩ. (c) Measured and simulated values for Re[Z] and Img[Z]from the model of RC. (d) Impedance spectrum of different samples changed with current amplitude. (e)Impedance

spectrum acquired, the black solid line is obtained from the model of RC between 10 and125 kHz. (f) and (h) Cole–Cole plots of different samples are obtained at 1h and 20h. (g) and (i) The plot of average value of |Z| and Arg(Z) are changed with time in different samples. In here Samples (milk, orange juice, peach juice and tomato juice) inoculated with 10^5 cfu/mL bacterial concentrations.

3.2 Cole-cole graph analyses

Fig. 3(e) shows a typical spectrum obtained using the sensor on an electronic circuit with R=1 kΩ and C=2.2 μF. This finding demonstrates that the sensor provided excellent results with good fit to the Cole-Cole theory at all frequencies between 5 and 125 kHz. Minor discrepancies were observed above 150 kHz with sight deviations from the semi-circular fit.

Given phase angle change with the unit change of pH value,[42] before sensing bacterial concentration, pH value could be noted for reference. In this paper, each sample was maintained at pH= 5±1.

To determine the appropriate parameter to be monitored, impedance value Z and phase angle θ were measured for all considered cases. Thus, the phase angle θ is a reliable indicator in this study. The model of Z consists of capacitive and resistive components [41], which could be attributed to the incipient phase separation of the samples during measurement. Figs. 3(f) and 3(g) show two Cole-Cole plots of the electrical impedance imaginary (Z) versus real (Z) at initial time periods of 1 and 20 h. These plots are based on different samples subjected to a time series of AE activity recorded simultaneously with the AC-conductivity at different selected frequencies (10 Hz and 100 kHz). The Cole-Cole plot [Fig. 3(f)] exhibits strong resistance characteristics at the initial time leading to the impossible outcome of characteristic frequency. The Cole-Cole graph [Fig. 3(g)] consists of two superimposed depressed

semicircles and a tail at the low frequency range. The low-frequency tail at the right side of the plots is due to the undesirable electrode response result. The main complex impedance arc in the Cole-Cole plot observed at the arc at medium frequencies is ascribed to the grain boundary contribution.[43] In the present case, the contributions of measurements may be modelled via an equivalent circuit with two components in series, each consisting of a CPE connection with a resistance *R*. The CPE outcome could be equal to the bacterial concentration when it reaches a threshold value of 10^6 cfu/mL. Such equivalent circuit models were used to describe the electrical behavior of general bacterial concentration as a function of time.

The phase separation exhibits different effects on the interface and "bulk" properties of the sensors because it influences the solution conductivity more than the electrical properties of the electrode/solution interface. The real (*Z*) and imaginary (*Z*) are parts of the complex electrical impedance as a function of frequency during the sequential loading sine wave. Thus, the real (*Z*) becomes unsuitable for detecting bacterial concentration. By contrast, the imaginary (*Z*), essentially determined by interface characteristics, is insignificantly affected by the phase angle separation and exhibits a predictable behavior in all considered cases.

The system was used to prove determination the feasibility of bacterial contaminant in different samples. Nutrient media must then be added to the sample to allow the bacteria to reach the critical concentration of 10^6 cfu/mL. In summary, impedance method was shown to work in all appropriate cases. The four different samples (milk, orange juice, peach juice, and tomato juice) based on fruit or containing alcohol exhibited no significant bacterial growth because it was inhibited by high organic acid or alcohol in the product (former and latter case, respectively).

3.3 Detection of phase angle analyses

Typical values of dielectric loss angle δ and $|Z|$ extracted from our experimental data are shown in Fig. 3(g) and Fig. 3(i). These data, collected during 24 h assays, were obtained from different types of soft drinks with the same initial bacterial concentration of 10^5 cfu/mL. The average phase angle value changed with time when the biosensor was dipped into different samples (milk, orange juice, peach juice, and tomato juice) inoculated with the same percentage of bacterial concentrations [Fig. 3(g) and Fig. 3(i)]. The black, red, blue and green curves show the phase angle when the sensor was dipped into 10^5 cfu/mL each of milk, orange juice, peach juice and tomato juice. The plots demonstrate that the phase angle of the biosensor is remarkably different among the samples.

The change in electrical impedance could reflect the growth of bacterial communities. The present study focuses on improving the accuracy of phase angle using the RREF algorithm. The rate of the dielectric loss angle δ increases in response to the bacterial concentration. Although the curves are noisier and exhibit smoother features than those obtained using suitable dilution media, the time (DT) at which δ begins to increase can be accurately calculated by using an PC-implemented algorithm that effectively filters out the experimental. Fig. 4(a) shows the measured curve, as well as the fitting function in the case of δ for a 10^5 cfu/mL milk sample. Each measurement is averaged over eight signal periods, which resulted in an electrical parameter (impedance and phase angle) estimation with precision > 99%. Such algorithm is based on the shape of the experimental curves. Before the bacterial concentration reaches the critical threshold of 10^6 cfu/mL, δ exhibits (at most) a slightly positive or negative drift [Fig. 3(i)]. Alternatively, when the threshold concentration is reached, δ exhibits a steep increase. Thus, our algorithm approximates the measured δ curves. The specific algorithm for determining DT is defined. When the bacterial concentration reaches the threshold value, the δ values can be expressed as:

$$\delta(t) = A_2 + \frac{A_1 - A_2}{1 + e^{\frac{t - t_0}{dt}}} (A_1 < \delta < A_2)$$

Then the value DT is determined and it is assumed that: $DT=t_0$.

In the case of the four samples, δ allowed the reliable measurement of bacterial concentration. In terms of percent variation, the dielectric loss angle δ is plotted versus time for different samples inoculated with various concentrations of the diluting medium [Fig. 4(a)]. The electrical parameters start to deviate from their baseline values at the time related to the initial bacterial concentration (higher contamination indicates lower DT). These parameters saturate when the bacterial population stabilizes. The stability of the population is attributed the cells, which no longer reproduce because of a lack of nutrients and the accumulation of toxic compounds in the media. The bacterial concentration upon electrical parameter saturation was approximately 10^8 cfu/mL using SPC and the value. The detection system must work independently to determine the possible presence of the unknown bacteria in the samples. Thus, a worst-case criterion must be adopted to discard samples contaminated by the slowest growing types of bacteria. Fig. 4(b) shows DT as a function of the initial microbial concentration for the different samples selected in this study. The linear regression line for the set of measures is $DT = -96.5 \text{ Log}_{10}(x) + 769$, and the coefficient of determination is $R^2 = 0.8581$ (the figure also shows the lower and higher limits of DT as functions of the microbial concentration inferred by Student *t*-distribution with a 95% confidence level).

The phase angle δ diversity exhibits an approximate growth from 0.02 to 0.36 in milk with different bacterial concentrations of [Fig. 4(c)]. The DT calculated from the δ curves is significantly different. Thus, the total time required to detect microbial concentration of more than 10^5 cfu/mL ranges from 5 h to 6 h, including 30 min of initial delay needed for the sample to reach the target temperature after the threshold microbial concentration was

418 properly calculated to determine DT. The DT of the black curves (10^5) is 296 min [Fig. 4(c)],
419 and those of the first (10^4), second (10^3) and third red curve (10^2) are 406,476 and 636 min,
420 respectively.

421 The dielectric loss angle δ exhibits an estimated growth from 0.02 to 0.38 in the orange
422 juice with different bacterial concentrations [Fig. 4(d)]. The DT of the black curves (10^5) is
423 292 min [Fig. 4(d)], and those of first (10^4), second (10^3), and third (10^2) red curves are 396,
424 506, and 592 min, respectively.

425 The dielectric loss angle δ exhibits growth from about 0.02 to 0.3 in peach juice with
426 different bacterial concentrations of [Fig. 4(e)]. The sugar concentration present in the
427 samples can decrease δ. The DT of the black curves (10^5) is 271 min [Fig. 4(e)], and those of
428 the first (10^4), second (10^3) and third (10^2) red curves are 321, 423 and 473 min, respectively.

429 The δ exhibits an approximate growth from 0.04 to 0.36 in tomato juice with different
430 bacterial concentrations of [Fig. 4(f)], and those of the first (10^4), second (10^3) and third (10^2)
431 red curves are 378, 458 and 650 min, respectively.

432 In summary, dealing with phase significantly adds sine-cosine sequence digital
433 demodulation based on an easy reference resistor circuit. The different growth rates δ(t) of
434 the dielectric loss angle could reflect the microbial concentration in 24 h. Efficient growth
435 media can support the recovery of stressed or injured bacterial cells. The test system was
436 suitable for applications in the industrial field (particularly in dairy products) as well as for
437 environmental monitoring (e.g. case of water microbial screening).

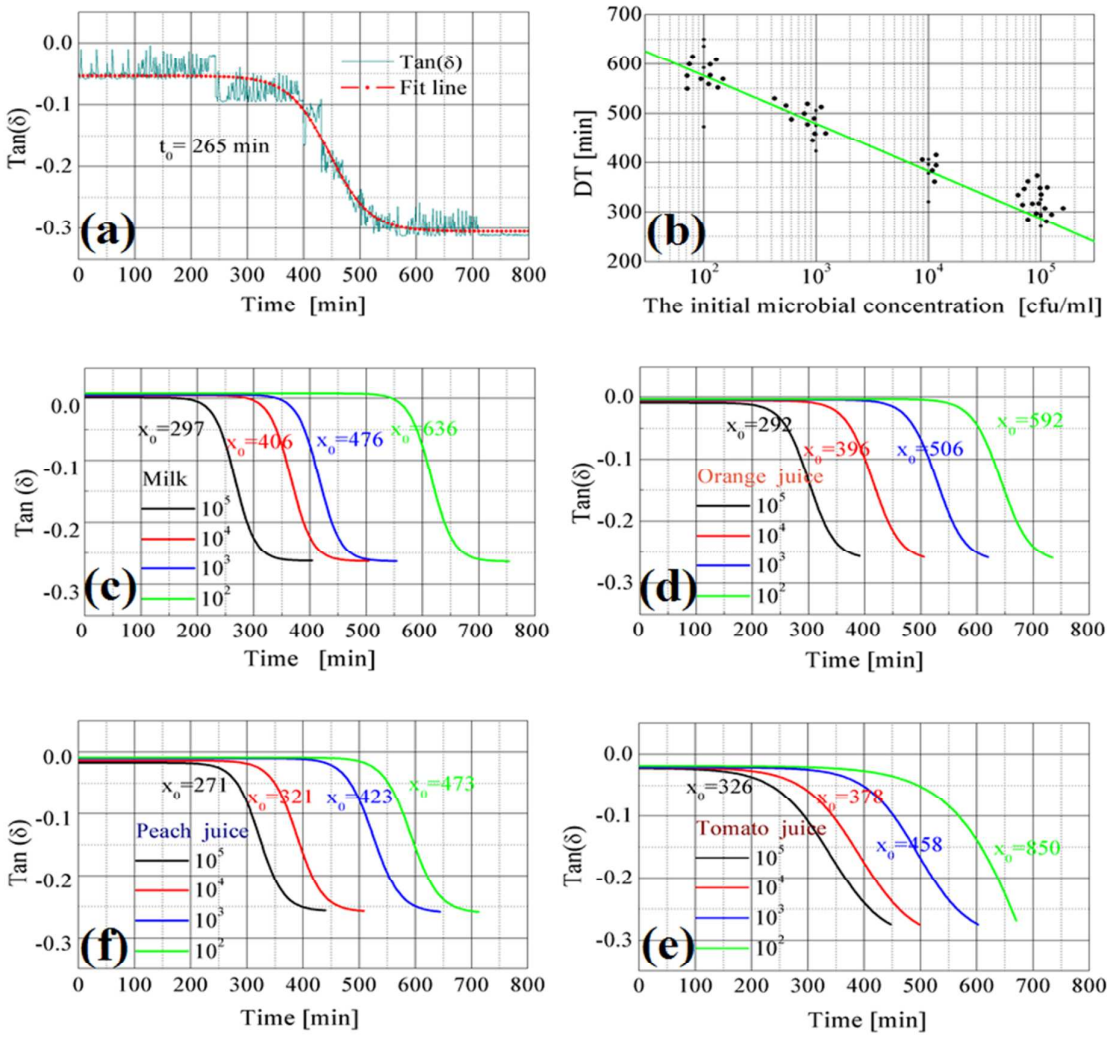

438

439 Fig. 4(a) Typical curve of the phase angle diversity δ and time with δ for best-fitting as a
440 function of the initial microbial concentration 105 cfu/mL milk sample. (b) Representation of
441 the DT obtained for the samples as a function of the initial microbial concentration (in log
442 scale). These data have been obtained with measurements at time intervals of 10 min during a
443 total time of 24 h. The samples have been incubated at a temperature of 39 ◦C. The obtained
444 regression line DT =-96.5 $Log_{10}(x)$ + 769 is also presented. The corresponding correlation
445 coefficient is R^2 = 0.8581. (c) Scatter plot representing DT as function of microbial
446 concentration and phase angle growth curves for milk samples inoculated with known
447 concentration. (d) Scatter plot representing DT as function of microbial concentration and

phase angle growth curves for orange juice samples inoculated with known concentration. (e) Scatter plot representing DT as function of microbial concentration and phase angle growth curves for peach juice samples inoculated with known concentration. (f) Scatter plot representing DT as function of microbial concentration and phase angle growth curves for tomato juice samples inoculated with known concentration.

4. Conclusion

In this study, a new type of portable biosensor system for determination bacterial concentration based on the change in value of dielectric loss angle δ was reported. As for competitiveness, this sensor provides more rapid results than standard plate count techniques (3 h for 10^6 cfu/mL) and avoids limited use in the laboratory. The system is a useful tool for microbial screening in the industrial field (in particular the dairy one is of interest here), as well as commercial environments.

Reference

1. C. Ruan, L. Yang and Y. Li, *Anal. Chem*., 2002, **74**, 4814.
2. H. J. Anders, V. Vielhauer, V. Eis, Y. Linde, M. Kretzler, G. P. de Lema, F. Strutz, S. Bauer, M. Rutz and H. Wagner, *The FASEB J.*, 2004, **18**, 534.
3. L. Ye and K. Mosbach, *Chem. Mater.*, 2008, **20**, 859.
4. K. Chang, S. Deng and M. Chen, *Biosens. Bioelectron*., 2014, **66**, 297.
5. T. S. Gunasekera, P. V. Attfield and D. A. Veal, *Appl. Environ. Microb.*, 2000, **66**, 1228.
6. M. Zourob, K. G. Ong, K. Zeng, F. Mouffouk and C. A. Grimes, *The Analyst*, 2007, **132**, 338.

7. S. Junya, H. Ryo, N. Daisuke, S. Masanori and H. Masanori, *J. Electrostat.*, 2003, **57**, 157.

8. T. A. Graubert, P. Cahan, D. Edwin, R. R. Selzer, T. A. Richmond, P. S. Eis, W. D. Shannon, X. Li, H. L. McLeod and J. M. Cheverud, *PLoS Genet.*, 2007, **3**, e3.

9. J. F. Drexler, A. Helmer, H. Kirberg, U. Reber, M. Panning, M. Müller, K. Höfling, B. Matz, C. Drosten and A. M. Eis-Hübinger, *Emerg. Infect. DIS.*, 2009, **15**, 1662.

10. J. J. Storhoff, S. S. Marla, P. Bao, S. Hagenow, H. Mehta, A. Lucas, V. Garimella, T. Patno, W. Buckingham and W. Cork, *Biosens. Bioelectron.*, 2004, **19**, 875.

11. L. Yang, Y. Li and G. F. Erf, *Anal. Chem.*, 2004, **76**, 1107.

12. S. Eustis and M. A. El-Sayed, *Chem. Soc. Rev.*, 2006, **35**, 209.

13. J. Homola, S. S. Yee and G. Gauglitz, *Sensor. Actuat. B: Chem.*, 1999, **54**, 3.

14. K. A. Willets and R. P. Van Duyne, *Annu. Rev. Phys. Chem.*, 2007, **58**, 267.

15. J. Homola, *Chem. Rev.*, 2008, **108**, 462.

16. K. Moxon, S. Hallman, A. Aslani, N. Kalkhoran and P. Lelkes, *J. Biomat. Sci-Polym. E.*, 2007, **18**, 1263.

17. M. R. Abidian and D. C. Martin, *Biomaterials*, 2008, **29**, 1273.

18. J. A. Davis, R. O. James and J. O. Leckie, *J. Colloid Interf. Sci.*, 1978, **63**, 480.

19. K. B. Oldham, *Journal of Electroanalytical Chemistry*, 2008, **613**, 131.

20. F. Silva, C. Gomes, M. Figueiredo, R. Costa, A. Martins and C. M. Pereira, *J. .Electroanal. Chem.*, 2008, **622**, 153.

21. S. J. Marrink, A. H. de Vries, T. A. Harroun, J. Katsaras and S. R. Wassall, *J. Am. Chem. Soc.*, 2008, **130**, 10.

22. A. A. Gurtovenko and J. Anwar, *J. Phys. Chem. B*, 2009, **113**, 1983.

23. S.R. Harroun. *Biochemistry*, 2006, **45**, 7090.

24. R. Sundararajan, *Mol. Biotechnol.*, 2009, **41**, 69.

25. M. Gajęcka and B. Przybylska-Gornowicz, *Pol. J. Vet. Sci.*, 2012, **15**, 711.
26. M. Grossi, M. Lanzoni, A. Pompei, R. Lazzarini, D. Matteuzzi and B. Riccò, *Biosens. Bioelectron.*, 2010, **26**, 983.
27. K. Maex, M. Baklanov, D. Shamiryan, S. Brongersma and Z. Yanovitskaya, *J. Appl. Phys.*, 2003, **93**, 8793.
28. J. C. Burfoot and G. W. Taylor, *Polar dielectrics and their applications*, Univ of California Press, 1979.
29. A. C. Metaxas and R. J. Meredith, Industrial microwave heating, IET, 1983.
30. G. G. Raju, *Dielectrics in electric fields*, CRC press, 2003, 3.
31. R. Coelho, *Physics of Dielectrics for the Engineer*, Elsevier, 2012.
32. D. Vanderbilt and R. King-Smith, *Phys. Rev. B*, 1993, **48**, 4442.
33. L. Beckmann, D. van Riesen and S. Leonhardt, *Conf. Proc. IEEE Eng. Med. Biol. Soc.* 2007, **2007**, 2685.
34. J. Agraz, A. Grunfeld, K. Cunningham, D. B. Li and S. Wagner, *J. Magn. Reson.*, 2013, **235**, 77.
35. J. F. M. Arguelles, M. A. Z. Arrieta, J. L. Dominguez, B. L. Jaurrieta and M. S. Benito, *Electr. Pow. Syst. Res.*, 2006, **76**, 194.
36. R. Bragós, J. Rosell and P. Riu, *Physiol. Meas.*, 1994, **15**, A91.
37. P. Bertemes-Filho, B. H. Brown and A. J. Wilson, *Physiol, Meas.*, 2000, **21**,1.
38. J. G. Chen, L. Feng and Y. H. Cheng, *Microelectron. Reliab.*, 2013, **53**, 129.
39. M. Grossi, M. Lanzoni, A. Pompei, R. Lazzarini, D. Matteuzzi and B. Ricco, *Biosens. Bioelectron.*, 2010, **26**, 983.
40. C. J. Felice, R. E. Madrid, J. M. Olivera, V. I. Rotger and M. E. Valentinuzzi, *J Microbiol. Meth.*, 1999, **35**, 37.
41. D. B. Stroud, B. H. Cornish, B. J. Thomas and L. C. Ward, *Clin. Nutr.*, 1995, **14**, 307.

42. D. M. Jenkins and M. J. Delwiche, *Biosens. Bioelectron.*, 2002, **17**, 557.

43. D. B. Stroud, B. H. Cornish, B. J. Thomas and L. C. Ward, *Appl. Radiat. Isotopes.*, 1998, **49**, 479.